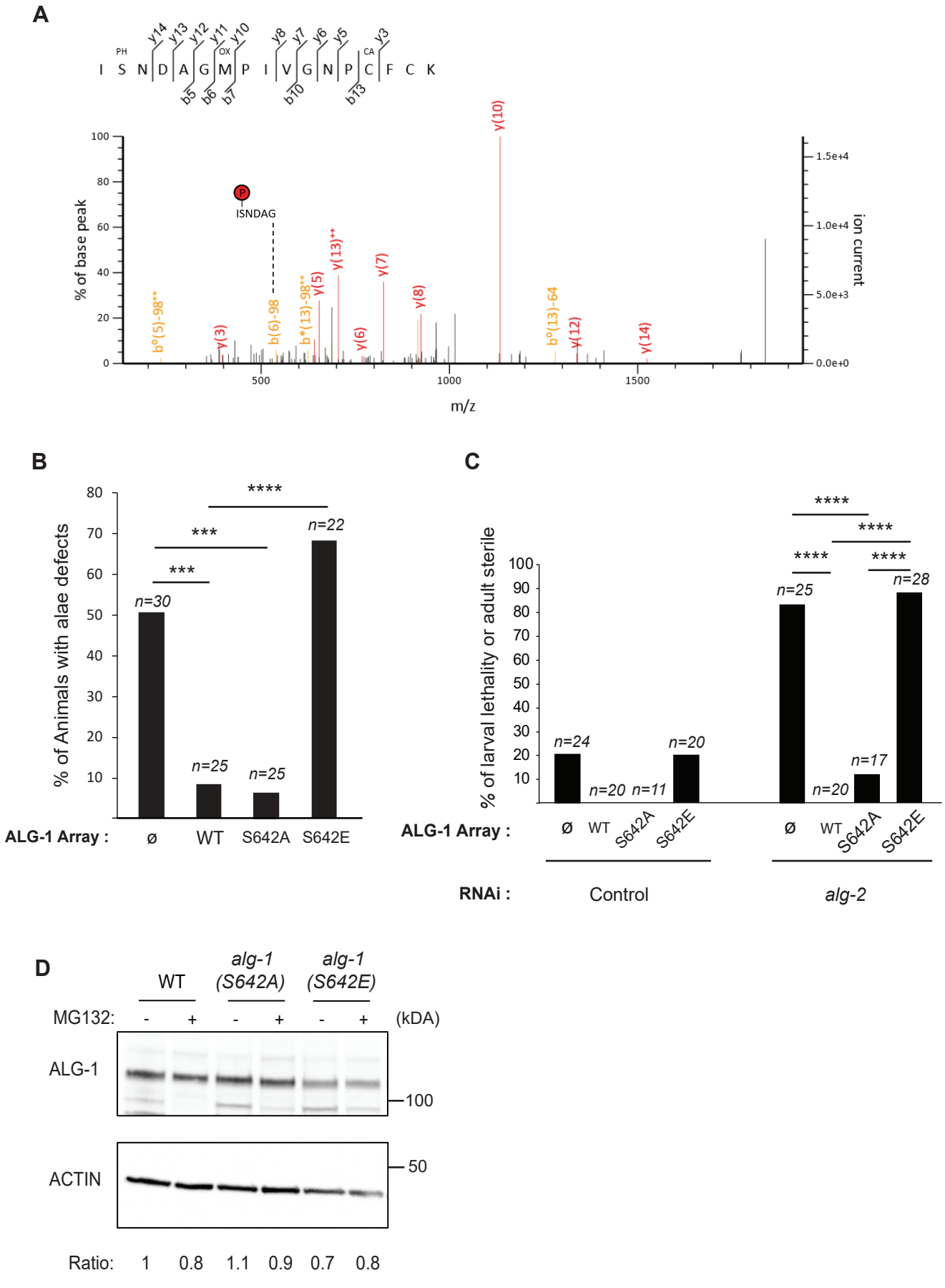
A
I S N D A G M P I V G N P C F C K
PH
OX
CA
ISNDAG
% of base peak
ion current
m/z
B
% of Animals with alae defects
n=30
n=25
n=25
n=22
***
***
****
ALG-1 Array :
ø
WT
S642A
S642E
C
% of larval lethality or adult sterile
n=24
n=20
n=11
n=20
n=25
n=20
n=17
n=28
****
****
****
****
ALG-1 Array :
RNAi :
Control
alg-2
D
WT
alg-1 (S642A)
alg-1 (S642E)
MG132:
(kDA)
ALG-1
ACTIN
100
50
Ratio: 1 0.8 1.1 0.9 0.7 0.8

Figure S1

Figure S1. Phosphorylation of ALG-1 serine 642 impairs the function of ALG-1.

(A) Representative CID fragment spectrum of a *C. elegans* ALG-1 peptide from a LC-UHR-QTOF run. Monophosphorylated ALG-1 peptide IpSNDAGMPIVGNPCFCK. Monoisotopic mass: 1917.78 Da, Mascot ion score: 21, Expectation value: 0.0089, Δ mass: -0.01 Da. Phosphosite localization at position 642 according to Mascot.

(**B**) *alg-1(0)* mutant animals carrying extrachromosomal transgene arrays of wild-type ALG-1 (WT), *alg-1(S642A)* or *alg-1(S642E)* were used to evaluate the ability of the transgenes to rescue the alae formation defects of *alg-1(0)* mutant animals. Young adult animals were monitored with Nomarski DIC microscopy to determine the structure of alae (complete or defective). The graph reports the fraction of animals with alae defect for each genotype. *P*-values were measured with a two-tailed Fisher's exact test, *** indicates $p<0.001$ and **** indicates $p<0.0001$. The sample size (n=) used for quantification is indicated.

(C) The same genotypes expressing transgenes of *alg-1* as in **(B)** were fed with bacteria that produce a control double-stranded RNA or double-stranded RNA containing *alg-2* sequence to trigger RNAi. The fraction of lethal or sterile adult animal for each transgenic strain is reported. *P*-values were measured with a two-tailed Fisher's exact test, *** indicates $p<0.001$ and **** indicates $p<0.0001$. The sample size (n=) used for quantification is indicated.

(D) Representative western blot of ALG-1 in wild type animals (WT), CRISPR-Cas9 edited non-phosphorylatable *alg-1(S642A)* and phospho-mimicking *alg-1(S642E)* mutants treated with proteasome inhibitor MG132 or only the vehicle (DMSO). Beta-Actin was used as a loading control. The ratio indicates the fold change compared to wild type ALG-1 (WT) treated with DMSO and normalized on Actin levels. Three replicates ($n=3$) of this experiment were used to calculate *P*-values with a Student's *t*-test and we report no significant difference in ALG-1 levels in worms treated with MG132 compared to only vehicle (DMSO). ALG-1 S642E levels were significantly lower than ALG-1 WT in both conditions (DMSO and DMSO+MG132) with an average fold change of 0.7 and *p*-values of 0.04 and 0.006 respectively.

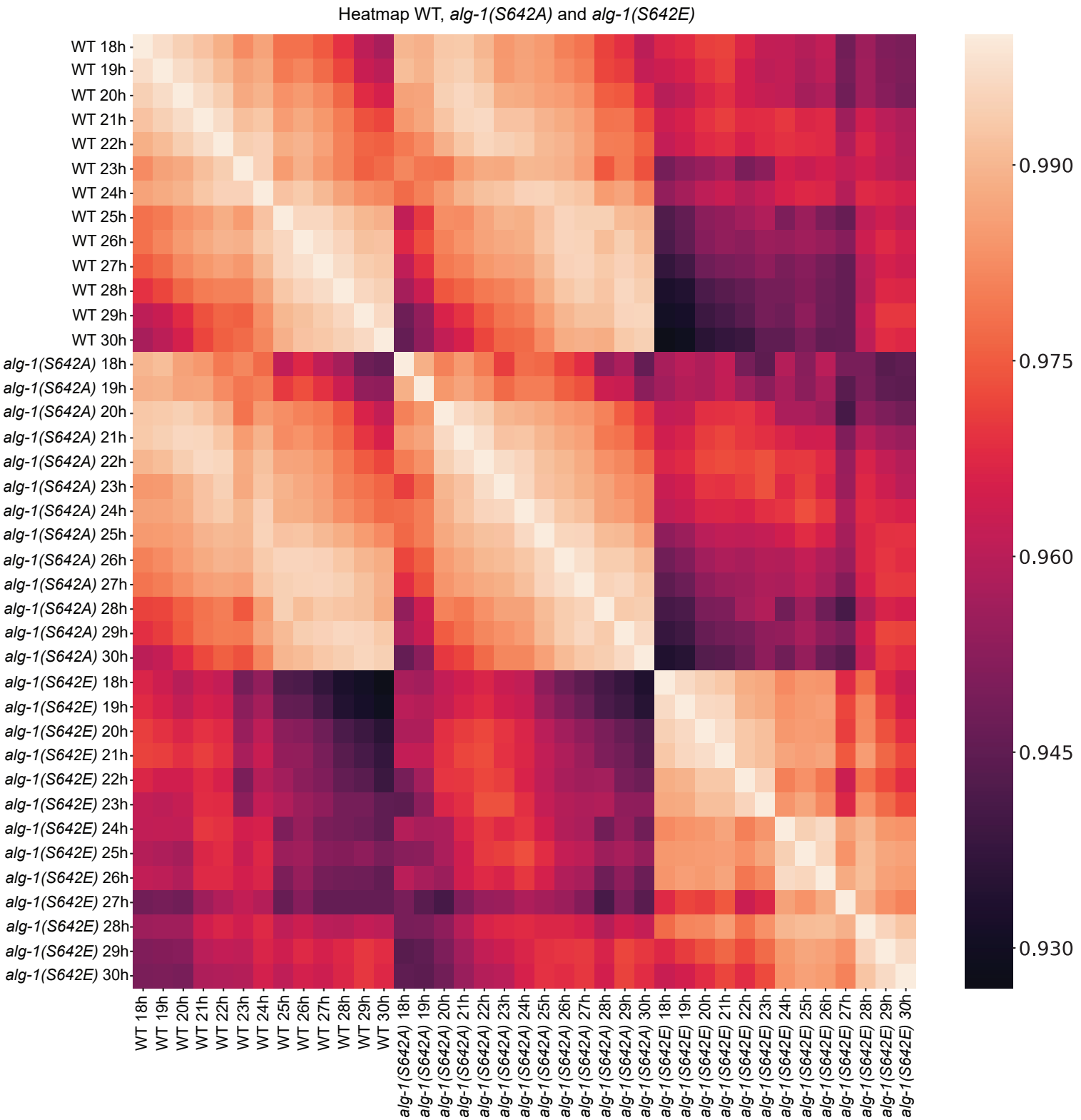
Heatmap WT, alg-1(S642A) and alg-1(S642E)
WT 18h
WT 19h
WT 20h
WT 21h
WT 22h
WT 23h
WT 24h
WT 25h
WT 26h
WT 27h
WT 28h
WT 29h
WT 30h
alg-1(S642A) 18h
alg-1(S642A) 19h
alg-1(S642A) 20h
alg-1(S642A) 21h
alg-1(S642A) 22h
alg-1(S642A) 23h
alg-1(S642A) 24h
alg-1(S642A) 25h
alg-1(S642A) 26h
alg-1(S642A) 27h
alg-1(S642A) 28h
alg-1(S642A) 29h
alg-1(S642A) 30h
alg-1(S642E) 18h
alg-1(S642E) 19h
alg-1(S642E) 20h
alg-1(S642E) 21h
alg-1(S642E) 22h
alg-1(S642E) 23h
alg-1(S642E) 24h
alg-1(S642E) 25h
alg-1(S642E) 26h
alg-1(S642E) 27h
alg-1(S642E) 28h
alg-1(S642E) 29h
alg-1(S642E) 30h
0.990
0.975
0.960
0.945
0.930

Figure S2

Figure S2. Heatmap of miRNA expression during development.

Pairwise correlation matrix heatmap of the log2 transformed values of miRNA expression (Pearson's correlation, shown in the legend on right) obtained by small-RNA sequencing in wild-type (WT), *alg-1(S642A)* and *alg-1(S642E)* animals grown from 18h to 30h at 25°C. At each timepoint, 1500 worms were plated for each sample. Each sample was divided by the total number of reads and multiplied by the average library size. Log2 expression levels were calculated after adding a pseudocount of 8.

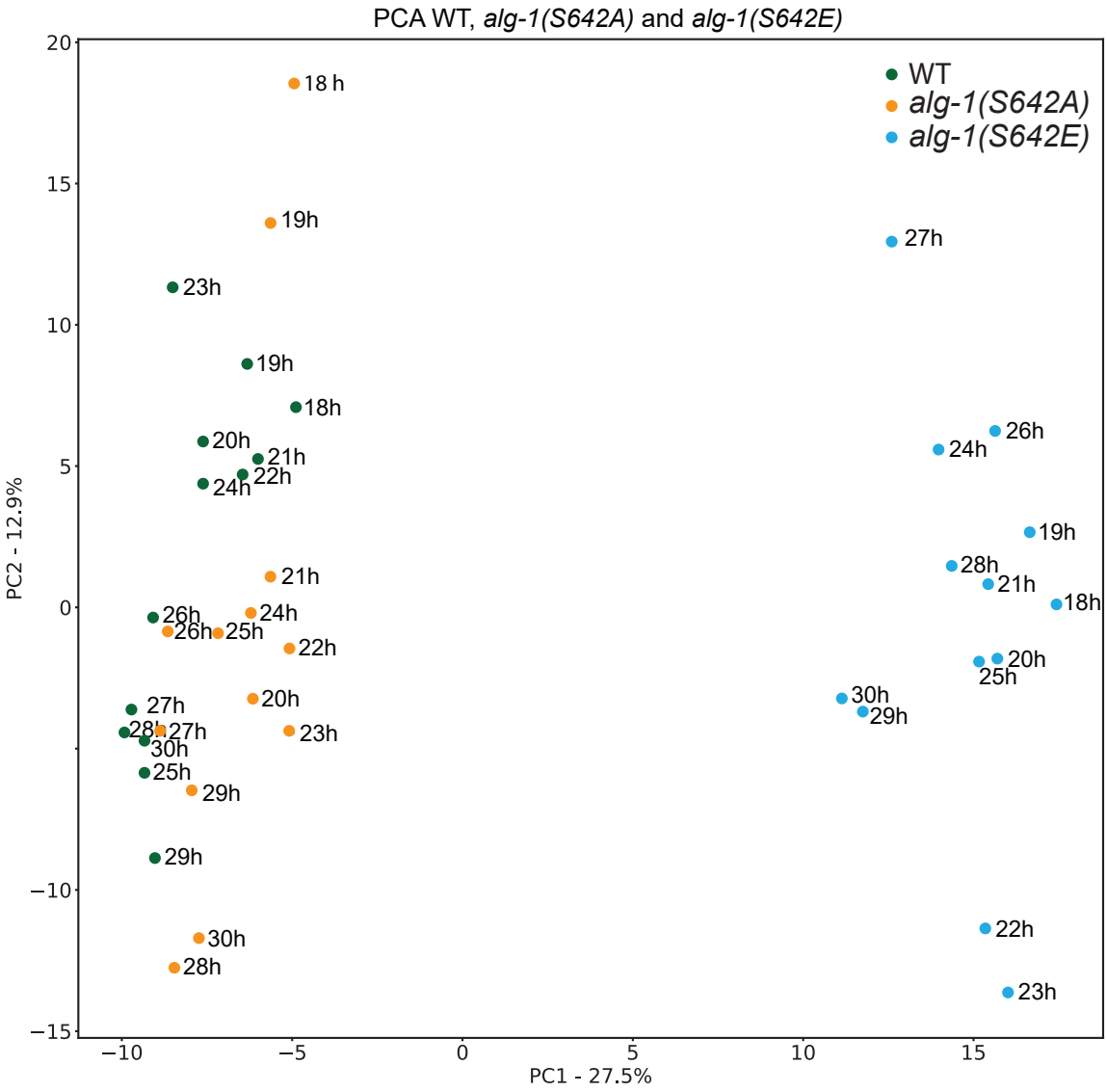
PCA WT, alg-1(S642A) and alg-1(S642E)
WT
alg-1(S642A)
alg-1(S642E)
PC1 - 27.5%
PC2 - 12.9%
18 h
19h
23h
19h
18h
20h
21h
22h
24h
21h
26h
24h
26h
25h
22h
20h
27h
28h
27h
30h
25h
29h
23h
29h
30h
28h
27h
26h
24h
19h
28h
21h
18h
20h
25h
30h
29h
22h
23h

Figure S3

Figure S3. Principal Component Analysis.

Principal Component Analysis (PCA) based on miRNA expression of samples wild-type (WT), alg-1(S642A) and alg-1(S642E) grown from 18 h to 30 h at 25°C (n=1500, each timepoint per sample). Samples with similar miRNA expression profiles are clustered together. The x and y axes indicate the percentage of explained variance of the first and second principal components, respectively.

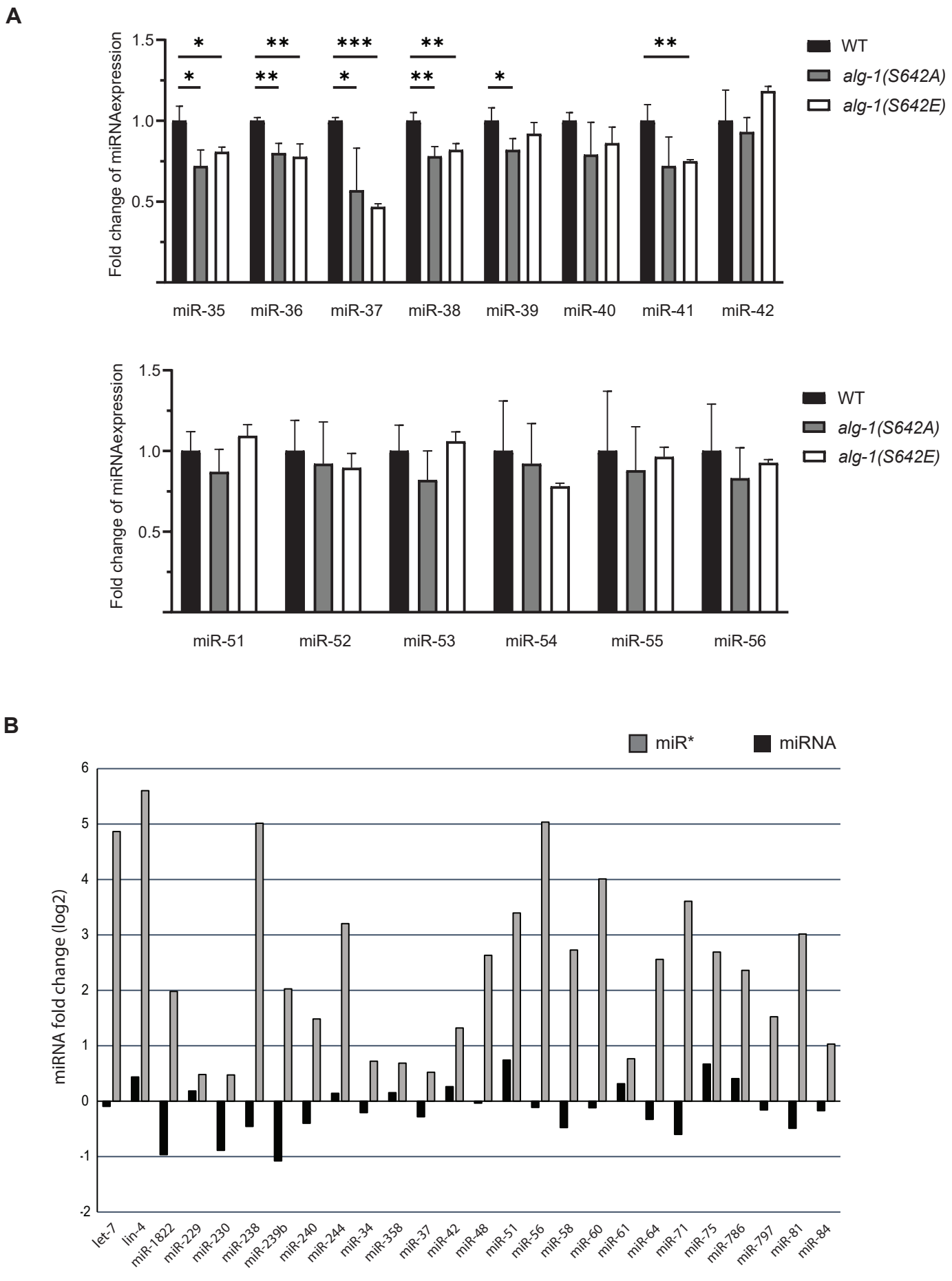
A
Fold change of miRNAexpression
1.5
1.0
0.5
WT
alg-1(S642A)
alg-1(S642E)
miR-35
miR-36
miR-37
miR-38
miR-39
miR-40
miR-41
miR-42
miR-51
miR-52
miR-53
miR-54
miR-55
miR-56
B
miR*
miRNA
miRNA fold change (log2)
6
5
4
3
2
1
0
-1
-2
let-7
lin-4
miR-1822
miR-229
miR-230
miR-238
miR-239b
miR-240
miR-244
miR-34
miR-358
miR-37
miR-42
miR-48
miR-51
miR-56
miR-58
miR-60
miR-61
miR-64
miR-71
miR-75
miR-786
miR-797
miR-81
miR-84

Figure S4

Figure S4. miR-35-42 and miR-51-56 miRNA families quantification in embryo and comparative guide and passenger strand expression in adults.

(A) RT-qPCR quantification of miR-35-42 and miR-51-56 miRNA family in embryos. Embryos were harvested from synchronised adult populations by alkaline hypochlorite solution treatment and incubated at room temperature for 4 hours in M9 solution with rotation before RNA extraction. The levels of the guide strands of miR-miR-35-42 miRNAs **(Top)** and miR-51-56 miRNAs **(Bottom)** in *alg-1(S642A)* and *alg-1(S642E)* embryos were measured by RT-pPCR and normalized to the levels measured in wild type embryos. Small nucleolar RNA sn2841 was used as an internal control gene. The error bars represent the 95% confidence interval from three biological replicates and the *p*-values were calculated using a two-tailed Student's *t*-test; *: $p<0.05$ and **: $p<0.01$.

(B) Fold change of normalized miRNA sequencing reads per million, expressed in $\log_2$, for both the guide (miRNA) and passenger strands (miR*) miRNAs in *alg-1(S642E)* mutants compared to wild type adult animals. The normalized reads per million were averaged over three biological replicates and miRNAs for which an increase in passenger strand was measured in adult animals are shown.

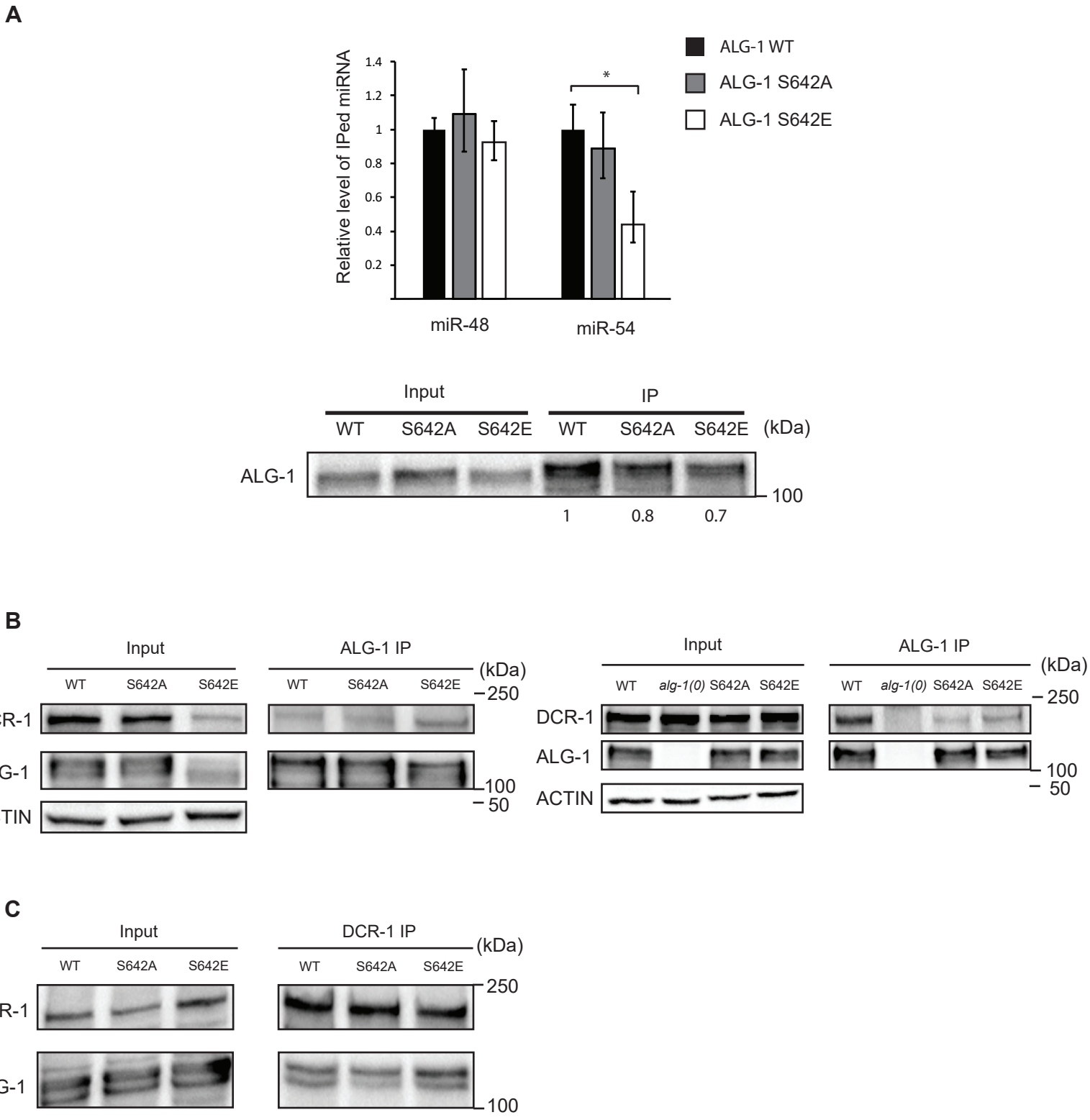
A
ALG-1 WT
ALG-1 S642A
ALG-1 S642E
Relative level of IPed miRNA
1.4
1.2
1
0.8
0.6
0.4
0.2
*
miR-48
miR-54
Input
IP
WT
S642A
S642E
WT
S642A
S642E
(kDa)
ALG-1
100
1
0.8
0.7
B
Input
ALG-1 IP
WT
S642A
S642E
WT
S642A
S642E
(kDa)
250
DCR-1
ALG-1
ACTIN
100
50
Input
ALG-1 IP
WT
alg-1(0)
S642A
S642E
WT
alg-1(0)
S642A
S642E
(kDa)
250
DCR-1
ALG-1
ACTIN
100
50
C
Input
DCR-1 IP
WT
S642A
S642E
WT
S642A
S642E
(kDa)
250
DCR-1
ALG-1
100

Figure S5

Figure S5. RT-qPCR of miRNAs associated to ALG-1 and DCR-1 Co-immunoprecipitation.

(A) ALG-1 immunoprecipitation (IP) from adult animal populations expressing either wild type *alg-1 (wt), alg-1(S642A) or alg-1(S642E)* were performed using a specific ALG-1 polyclonal antibody. **Top**: 90% of immunoprecipitated complexes were used to detect levels of miRNAs by quantitative RT-qPCR. Samples were spiked-in with human miR-20a miRNA before RNA purification and used as a technical control. The error bars represent the 95% confidence interval from three biological replicates, * indicates the statistical significance obtained from a Student's *t*-test $p<0.05$. **Bottom**: Representative image of a western blot of ALG-1 IP for miRNA quantification. 10% of the immunoprecipitated ALG-1 complex was used to detect ALG-1 by western blot. The input is 10% of protein extract used for immunoprecipitation. The ALG-1 levels in the IP relative to the signal of WT are shown and miRNA quantification was further normalized according to these values.

(B) ALG-1 and DCR-1 co-IP. The interaction between ALG-1 (WT, S642A and S642E) and DCR-1 was evaluated by ALG-1 IP in adult animal extracts. Two biological replicates are shown. *alg-1(0)* animals (right panel) were used as a control.

(C) ALG-1 and DCR-1 co-IP. The interaction between ALG-1 (WT, S642A and S642E) and DCR-1 was evaluated by DCR-1 IP in embryo extracts. One biological replicate was performed.

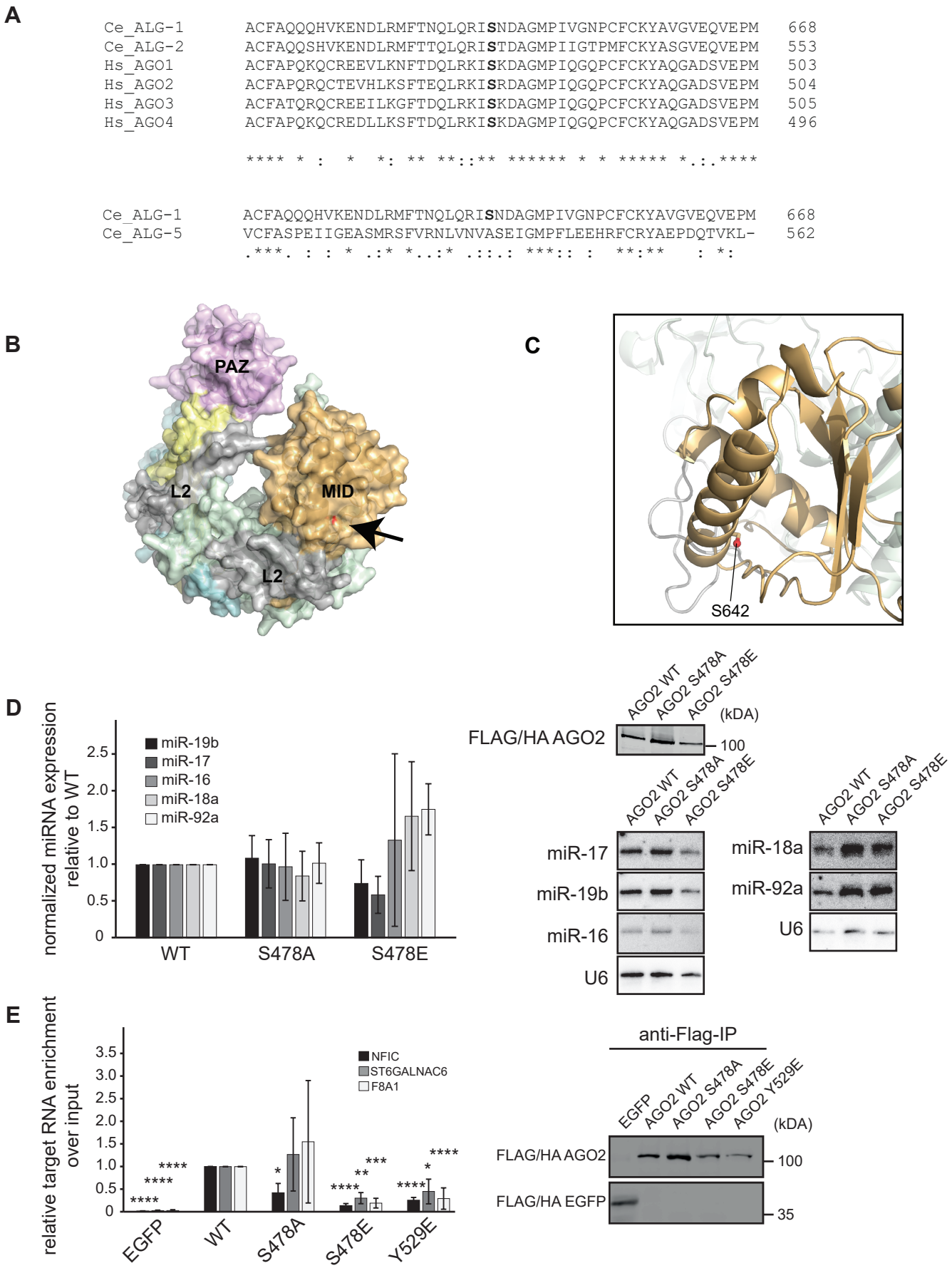
A
Ce_ALG-1 ACFAQQQHVKENDLRMFTNQLQRISNDAGMPIVGNPCFCKYAVGVEQVEPM 668
Ce_ALG-2 ACFAQQSHVKENDLRMFTTQLQRISTDAGMPIIGTPMFCKYASGVEQVEPM 553
Hs_AGO1 ACFAPQKQCREEVLKNFTDQLRKISKDAGMPIQGQPCFCKYAQGADSVEPM 503
Hs_AGO2 ACFAPQRQCTEVHLKSFTEQLRKISRDAGMPIQGQPCFCKYAQGADSVEPM 504
Hs_AGO3 ACFATQRQCREEILKGFTDQLRKISKDAGMPIQGQPCFCKYAQGADSVEPM 505
Hs_AGO4 ACFAPQKQCREDLLKSFTDQLRKISKDAGMPIQGQPCFCKYAQGADSVEPM 496
Ce_ALG-1 ACFAQQQHVKENDLRMFTNQLQRISNDAGMPIVGNPCFCKYAVGVEQVEPM 668
Ce_ALG-5 VCFASPEIIGEASMRSFVRNLVNVASEIGMPFLEEHRFCRYAEPDQTVKL- 562
B
PAZ
L2
MID
L2
C
S642
D
normalized miRNA expression relative to WT
miR-19b
miR-17
miR-16
miR-18a
miR-92a
WT
S478A
S478E
AGO2 WT
AGO2 S478A
AGO2 S478E
(kDA)
FLAG/HA AGO2
100
miR-17
miR-19b
miR-16
U6
miR-18a
miR-92a
U6
E
relative target RNA enrichment over input
NFIC
ST6GALNAC6
F8A1
EGFP
WT
S478A
S478E
Y529E
anti-Flag-IP
AGO2 Y529E
FLAG/HA AGO2
FLAG/HA EGFP
35

Figure S6

Figure S6. Sequence alignment, accessibility on the apo ALG-1 structure and analysis of human AGO2 serine 478 mutants.

(A) Top: Sequence alignment of *C. elegans* miRNA-specific and four human AGO proteins. Alignment of *C. elegans* ALG-1 and ALG-2 and human AGO1-4 using Clustal Omega. **Bottom:** Sequence alignment of *C. elegans* Argonaute ALG-1 and ALG-5 using Clustal Omega.

(B) Overall structure of ALG-1 shown as a surface model.

(C) The side chain of serine 642 is depicted as a ball and stick model. The hydroxyl oxygen of S642 is colored in red. For clarity, the N-terminal extended region and the insertion in the L2 domain unique to ALG-1 are not shown.

(D) miRNA quantification in cells expressing AGO2 serine 478 phosphorylation mutants. Flag/HA-tagged AGO2 WT or Flag/HA-tagged AGO2 serine 478 (the conserved serine corresponding to ALG-1 serine 642) mutated into alanine (S478A) or glutamate (S478E) were transfected in HEK 293T cells to quantify miRNA expression with Northern blotting. miRNA signals were normalized to corresponding U6 snRNA signal and compared to WT expression. **Left:** Average miRNA expression in cells transfected with AGO2 S478A and AGO2 S478E relative to AGO2 WT. Three biological replicates were used for quantification ($n=3$) and calculated as mean. Error bars represent the standard deviation. p-values were calculated using a two-tailed Student's *t*-test and no significant difference between wild type AGO2 and mutant AGO2 was observed. **Top right:** Western blot showing representative Flag/HA AGO2 expression with HA antibody. **Bottom right:** Representative Northern blots of miR-17, miR-19b, miR-16, miR-18a, miR-92a and U6 used for quantification.

(E) RIP experiment to analyse AGO2 mRNA target binding. HEK 293T cells were transfected with FLAG/HA-tagged AGO2 WT or with FLAG/HA-tagged AGO2 mutants S478A, S478E and Y529E. AGO2 Y529E was used as a control because it disrupts miRNA binding[S1]. Flag-tagged proteins were immunoprecipitated, bound RNA was extracted, and cDNA was synthesized. Target binding of AGO2 WT and mutants was analyzed by qRT-PCR. EGFP served as a negative control. Data was analyzed with the ΔΔCt method as relative enrichment over input. The values were normalized to the relative amount of immunoprecipitated AGO2 protein as determined with HA antibody by Western blotting. Analysis was performed with three biological replicates and calculated as mean. Error bars represent the standard deviation. *: $p<0.05$, **: $p<0.01$, ***: $p<0.001$ and ****: $p<0.0001$ as determined with a two-tailed Student's *t*-test.

SUPPLEMENTAL INFORMATION

Table S1. Residue accessibility of the corresponding serine 642 on the human AGO1-4 structures.

The table reports if residues corresponding to ALG-1 serine 642 on human Argonautes are solvent-exposed or buried within the structure, based on published crystal structures of the human AGO1-4. The table discriminates AGO structures that are bound to a miRNA (RISC) and AGO structures that are bound to a target RNA (Target-bound RISC). The table shows the identifier for the structure in the Protein Data Bank (PDB ID), the human Argonaute (AGO1-4), the availability of the serine on the structure (exposed or buried), the reference of the published structure and the number of molecules in the crystallographic Asymmetric Structure (ASU) (# of mol/ASU).

RISC

PDB ID	AGO	Ser corresponding to S642	Reference	# of mol/ASU
4XKT	1	exposed	[S2]	1
4KRE	1	exposed	[S3]	1
4KRF	1	buried	[S3]	1
4OLA	2	buried	[S4]	1
4F3T	2	buried	[S5]	1
4W5N	2	buried	[S6]	1
5VM9	3	buried	[S7]	2
6OON	4	buried	[S8]	1

Target-bound RISC

PDB ID	AGO	Ser corresponding to S642	Reference	# of mol/ASU
4W5O	2	exposed	[S6]	1
4W5Q	2	buried	[S6]	1
4W5R	2	buried	[S6]	1
4W5T	2	buried	[S6]	1
6N4O	2	buried	[S9]	1
6MFN	2	buried	[S10]	1
6MDZ	2	buried	[S10]	2
6MFR	2	buried	[S10]	2
6NIT	2	buried	[S10]	2

Table S2. Oligonucleotides used in this study.

Site directed mutagenesis		
Name	**Target: modification**	**Sequence**
mso2792	*alg-1: alg-1(S642A)*	TCAGCGGATTgctAACGACGCTG
mso2793	*alg-1*	AGCTGGTTGGTGAACATG
mso2794	*alg-1: alg-1(S642E)*	TCAGCGGATTgaaAACGACGCTG
S478A-fwd	AGO2: AGO2(S478A)	CTCAGAAAGATCGCGAGAGACGCCG
S478A-rev	AGO2: AGO2(S478A)	CGGCGTCTCTCGCGATCTTTCTGAG
S478E fwd	AGO2: AGO2(S478E)	CAGCTCAGAAAGATCGAGAGAGACGCCGGCATG
S478E-rev	AGO2: AGO2(S478E)	CATGCCGGCGTCTCTCTCGATCTTTCTGAGCTG
Gene Editing CRISPR-Cas9		
crRNA	**Target to edit**	**Sequence + GUUUUAGAGCUAUGCUGUUUUG linker**
crRNA30	*alg-1(S642)*	UGUUCACCAACCAGCUUCAGGUUUUAGAGCUAUGCUGUUUUG
crRNA41	*alg-1(Y693)*	CCUGGAAAAACUCCAGUUUAGUUUUAGAGCUAUGCUGUUUUG
crRNA53	*kin-2(R92)*	GAGCCACCAAAGAGAUCAGGGUUUUAGAGCUAUGCUGUUUUG
ssODN (HDR template)	**Edit**	**Sequence**
ssODN32	*alg-1(S642A)*	TCAAGTACTTGAACATTGGCTCAACCTGCTCGACTCCAACAGC GTACTTGCAGAAGCATGGATTTCCGACGATTGGCATACCcGCG TCGTTggcAATgCGCTGAAGCTGGTTGGTGAACATGCGGAGATC GTTCTCCTTGACATGCTG
ssODN31	*alg-1(S642E)*	TCAAGTACTTGAACATTGGCTCAACCTGCTCGACTCCAACAGC GTACTTGCAGAAGCATGGATTTCCGACGATTGGCATACCcGCG TCGTTctcAATgCGCTGAAGCTGGTTGGTGAACATGCGGAGATC GTTCTCCTTGACATGCTG
ssODN56	*kin-2(R92C)*	TTGTACTCGGTATCGTCCTCCTTGATTGGTTCGGCAGAGATTCC GGTTCTGCATCCACCactTCTCTTTGGTGGCTCCACAATGATGTC GTCATCATCAGCAGCGTCCGG
RNAi		
cDNA target	**Strand**	**Sequence**
kin-2	forward	GCGAATTGGGTACCCATGTACGATGCCATGTTCC
kin-2	Reverse	CTGCCGCTCTAGACAGGATCTCACGAACTGGTC
2'-O-Methyl Pull-Down		
Target	**Sequence**	
miR-35	5′-Biotin-ucuucacugcuaguuuccacccggugaaccuu-3′	
luciferase (non-specific)	5′-Biotin-caucacguacgcggaauacuucgaaauguc-3′	
RT-qPCR		
Target	**Sequence**	
NFIC fwd	GACCTGTACCTGGCCTACTTTG	
NFIC rev	CACACCTGACGTGACAAAGCTC	

F8A1 fwd	GTTTGCGTCTGGGGAGGAAT
F8A1 rev	TGGTAACGTTCAGCCAACGA
ST6GALNAC6 fwd	CATTCGTGGTTGAGCACAGG
ST6GALNAC6 rev	CCGCTGGCTGCAGTAGTT

Data S1. The levels of let-7 family miRNAs are altered in *alg-1* serine 642 phosphorylation mutants.

Expression patterns of passenger strands (let-7-3p, miR-48-3p, miR-84-3p and miR-241-3p) and guide strands (let-7-5p, miR-48-5p, miR-84-5p and miR-241-5p) from the small-RNA seq of WT, *alg-1(S642A)* and *alg-1(S642E)* animals grown from 18h to 30 h at 25°C are plotted over time. At each timepoint, 1500 worms were plated for each sample. Read counts were normalized to reads per million and plotted in $\log_2$. The graph for each miRNA represents reads from one biological replicate per genotype, with measurement at multiple time points.

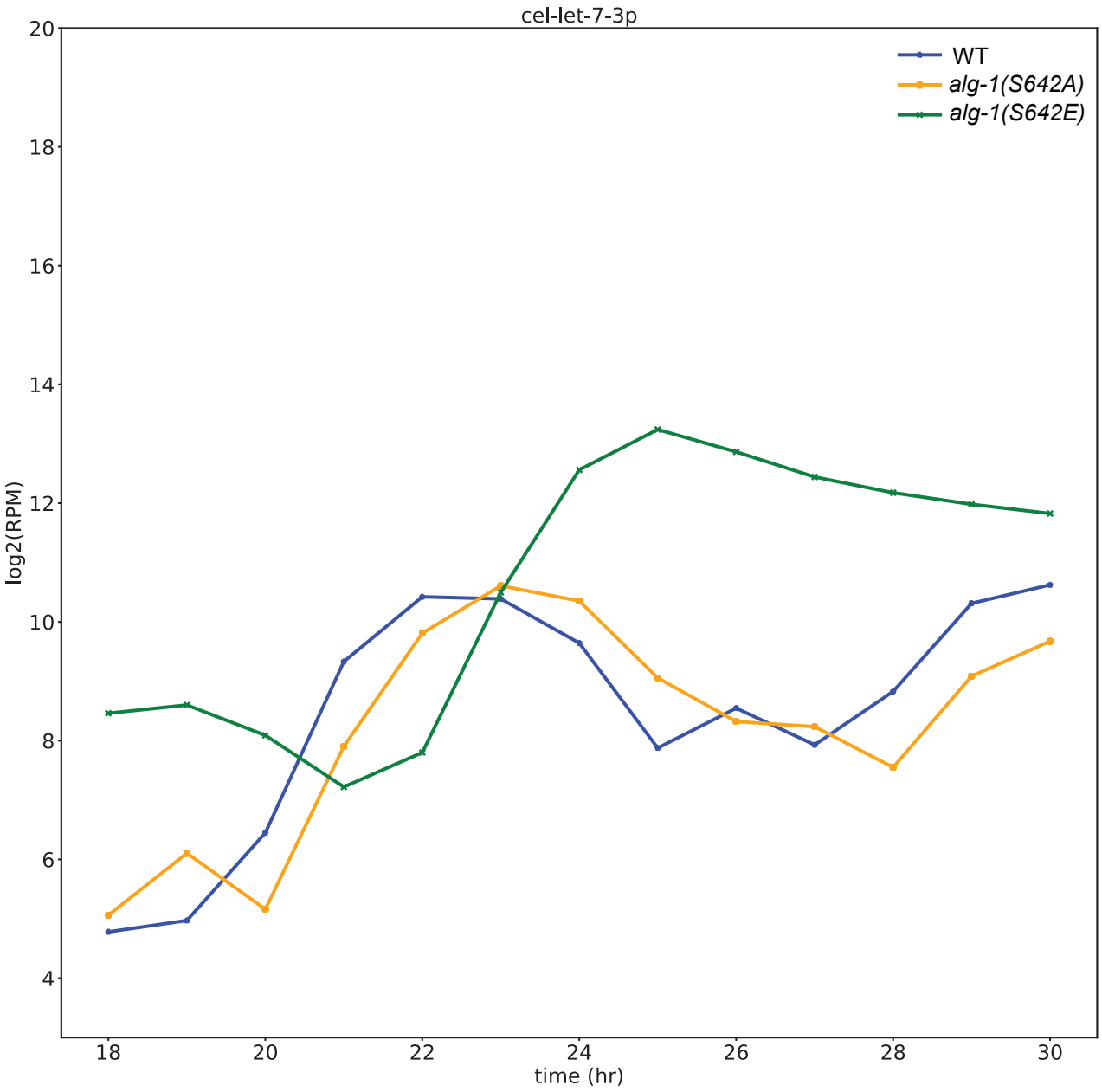
cel-let-7-3p
WT
alg-1(S642A)
alg-1(S642E)
log2(RPM)
time (hr)
20
18
16
14
12
10
8
6
4
18
20
22
24
26
28
30

Data S1

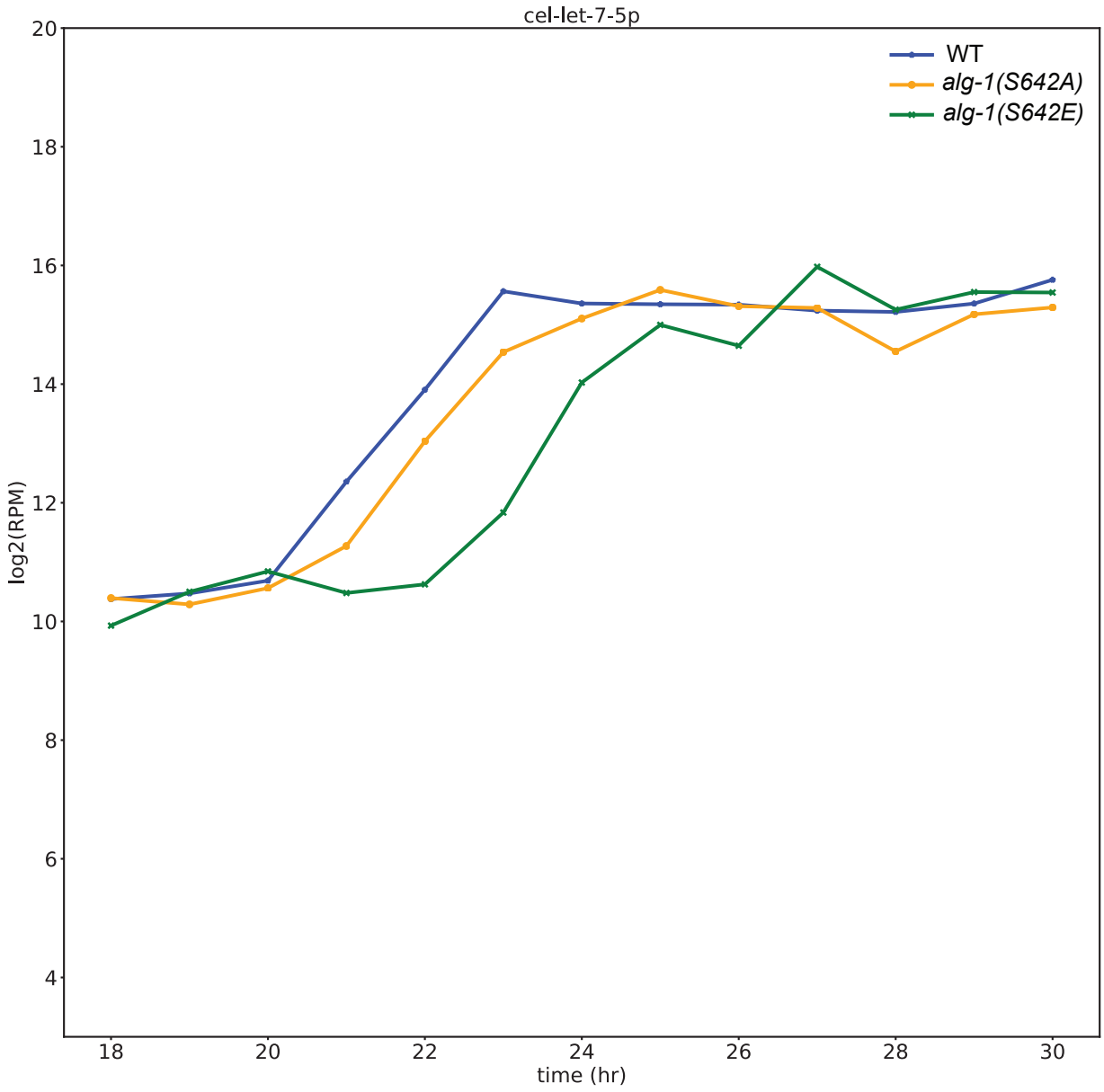
cel-let-7-5p
WT
alg-1(S642A)
alg-1(S642E)
log2(RPM)
time (hr)
20
18
16
14
12
10
8
6
4
18
20
22
24
26
28
30

Data S1

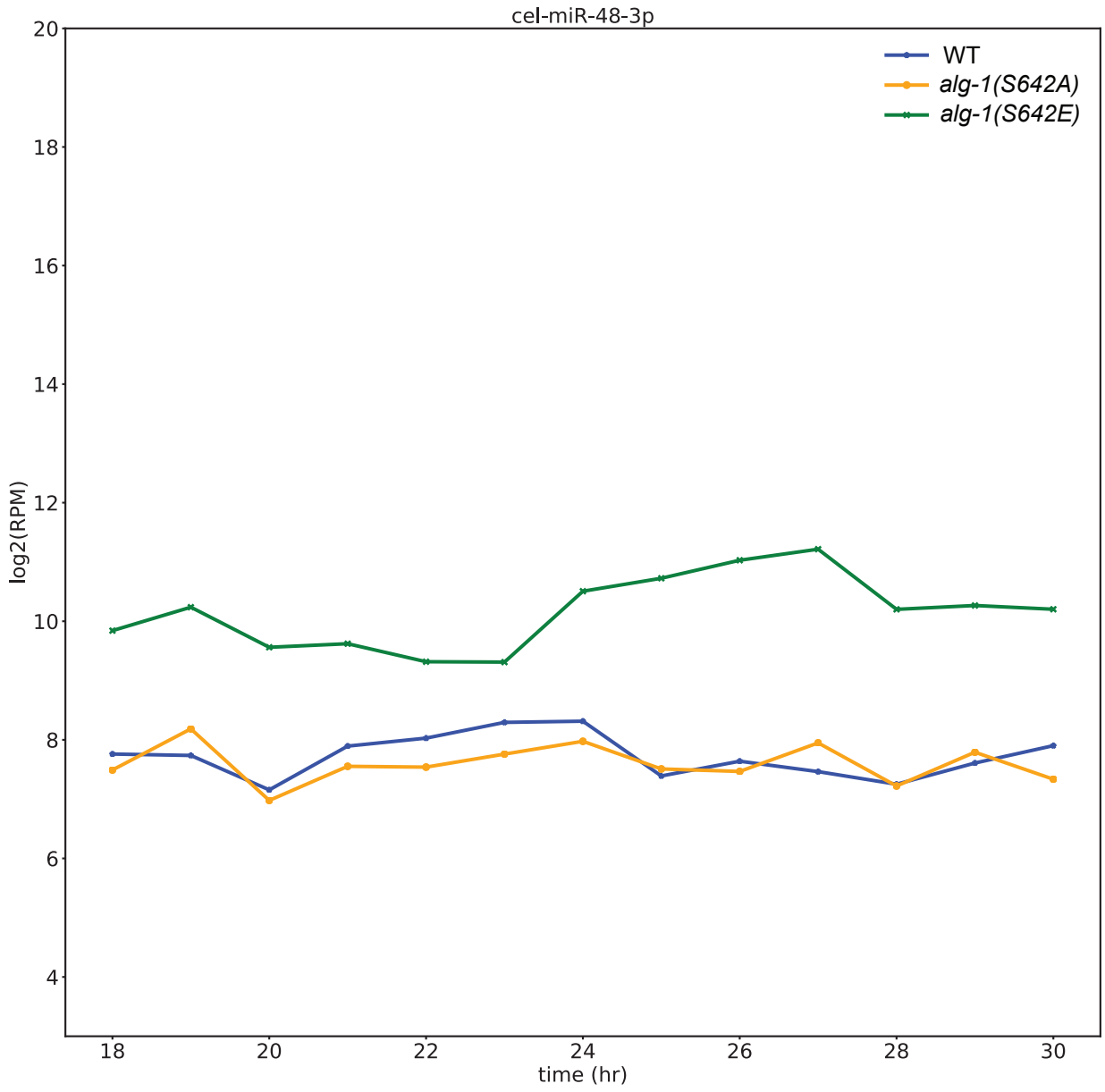
cel-miR-48-3p
WT
alg-1(S642A)
alg-1(S642E)
log2(RPM)
time (hr)
20
18
16
14
12
10
8
6
4
18
20
22
24
26
28
30

Data S1

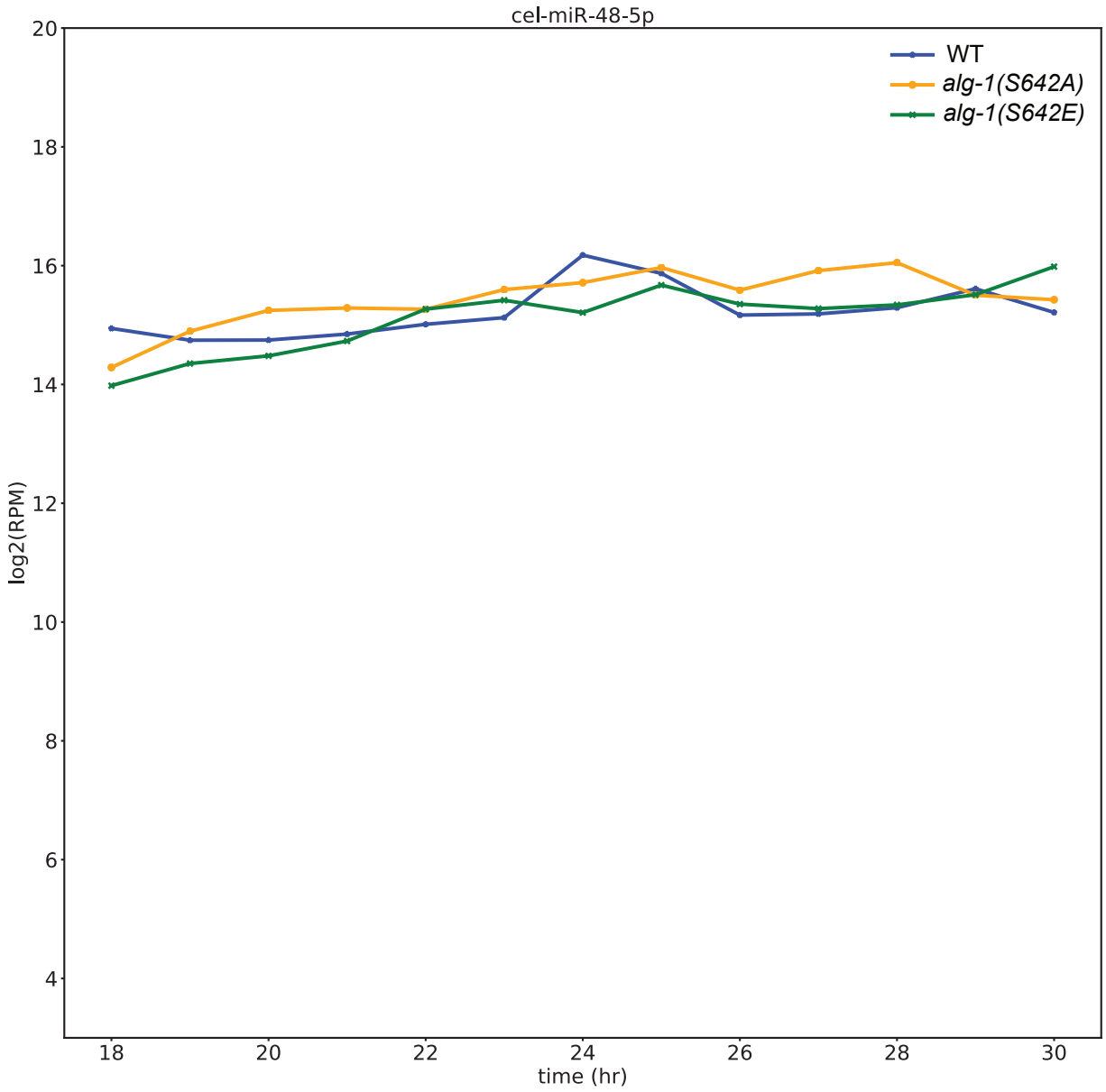
cel-miR-48-5p
WT
alg-1(S642A)
alg-1(S642E)
log2(RPM)
time (hr)
20
18
16
14
12
10
8
6
4
18
20
22
24
26
28
30

Data S1

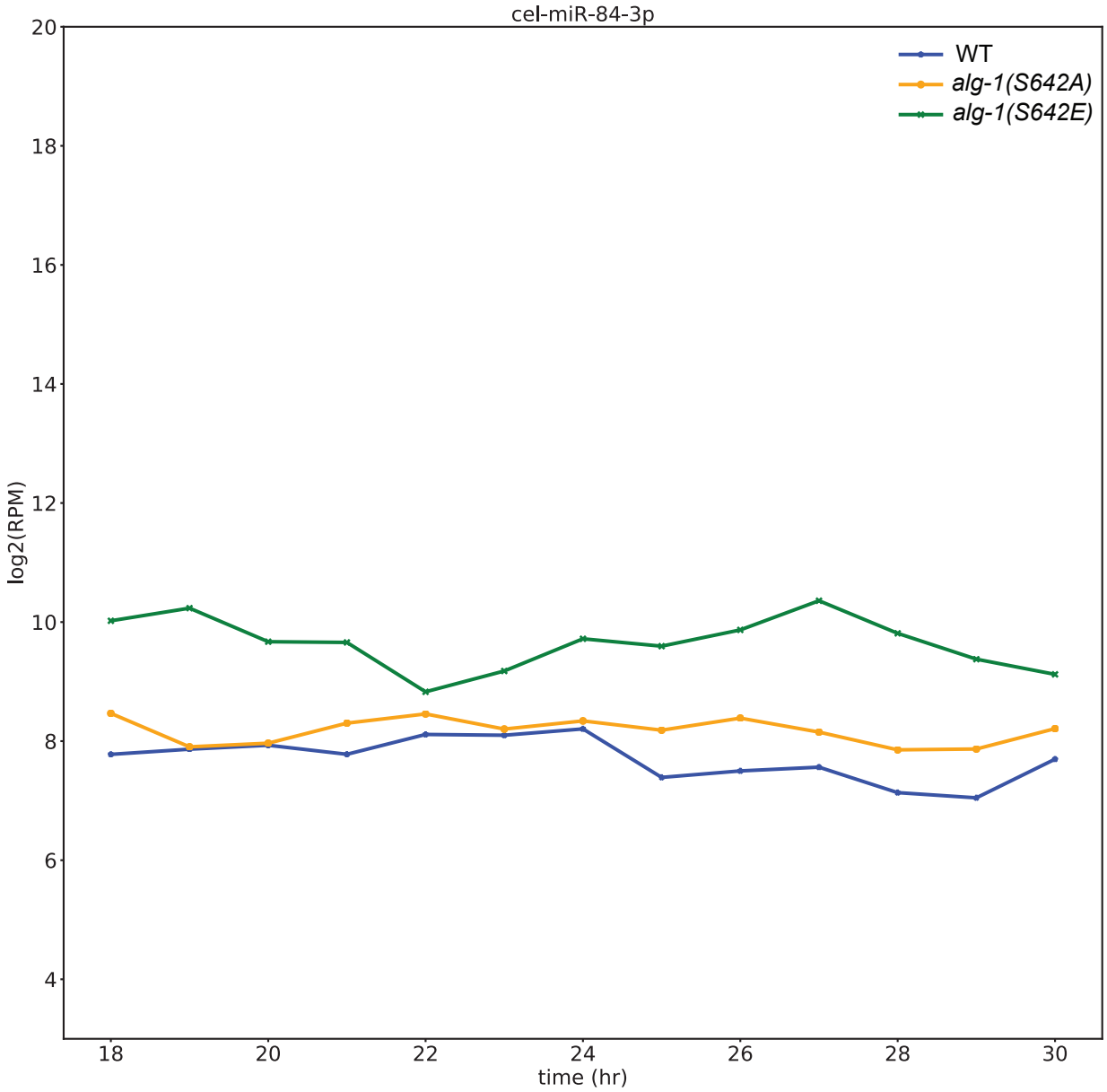
cel-miR-84-3p
WT
alg-1(S642A)
alg-1(S642E)
log2(RPM)
time (hr)
20
18
16
14
12
10
8
6
4
18
20
22
24
26
28
30

Data S1

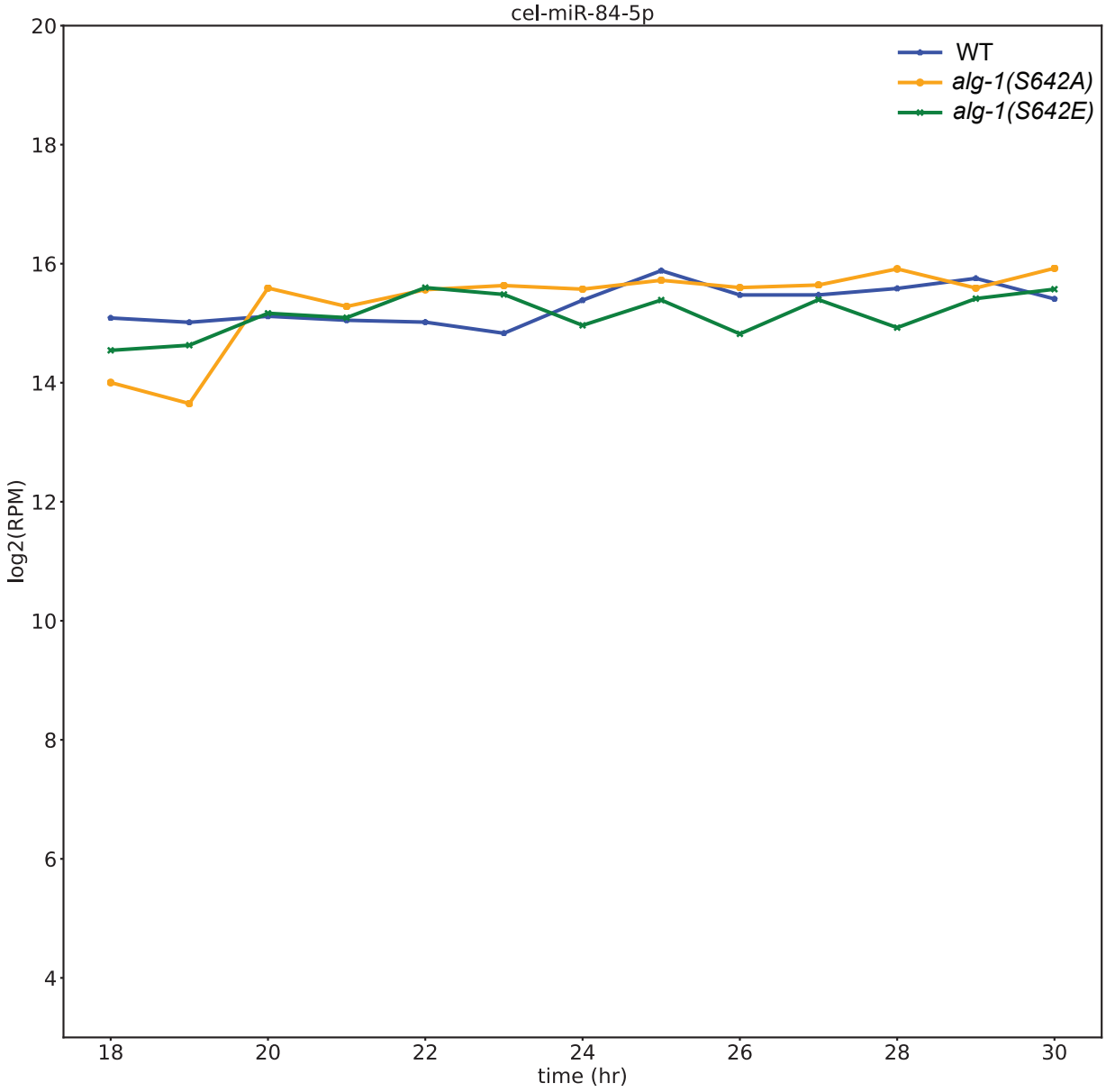
cel-miR-84-5p
WT
alg-1(S642A)
alg-1(S642E)
log2(RPM)
time (hr)
20
18
16
14
12
10
8
6
4
18
20
22
24
26
28
30

Data S1

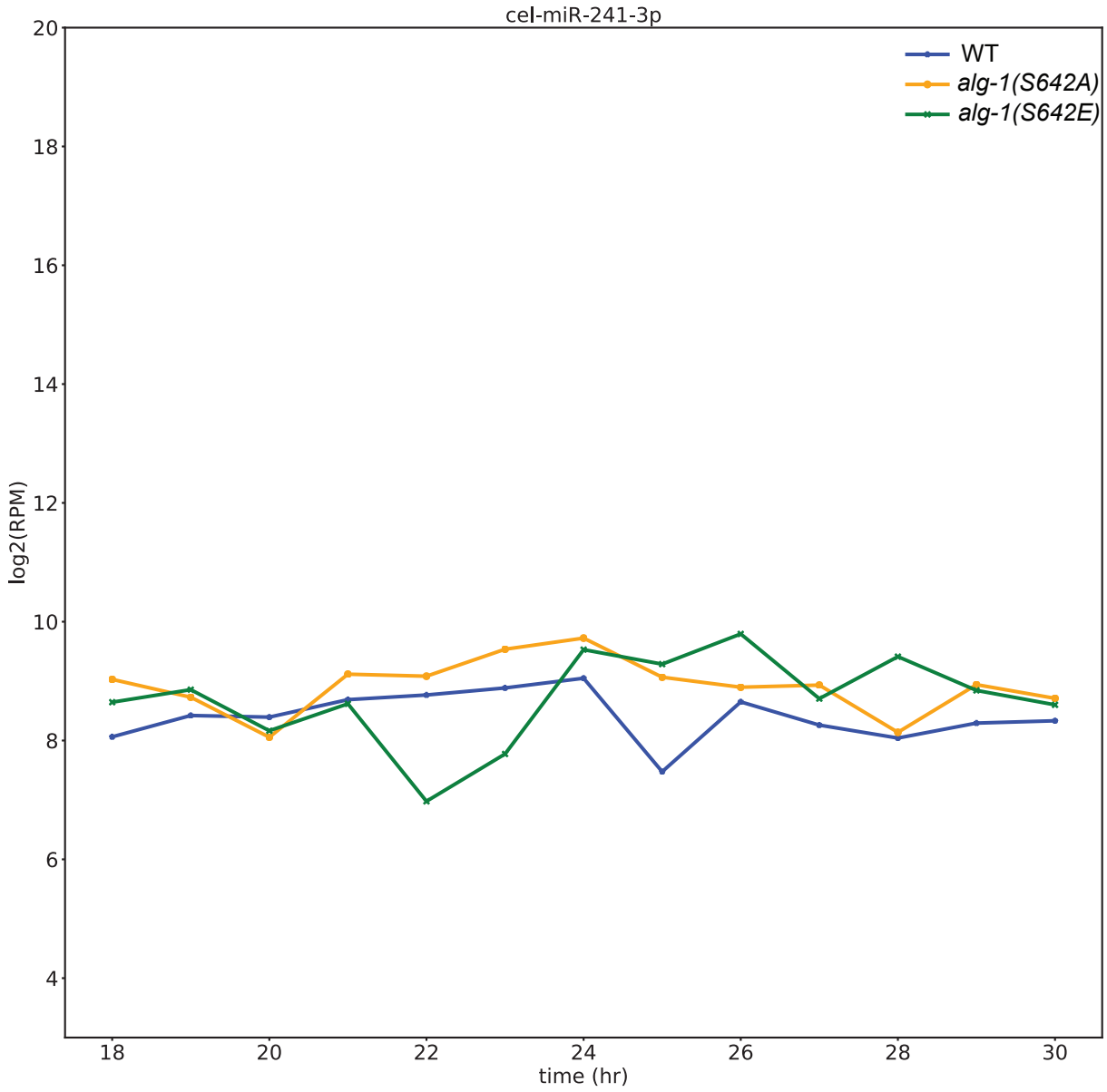
cel-miR-241-3p
WT
alg-1(S642A)
alg-1(S642E)
log2(RPM)
time (hr)
20
18
16
14
12
10
8
6
4
18
20
22
24
26
28
30

Data S1

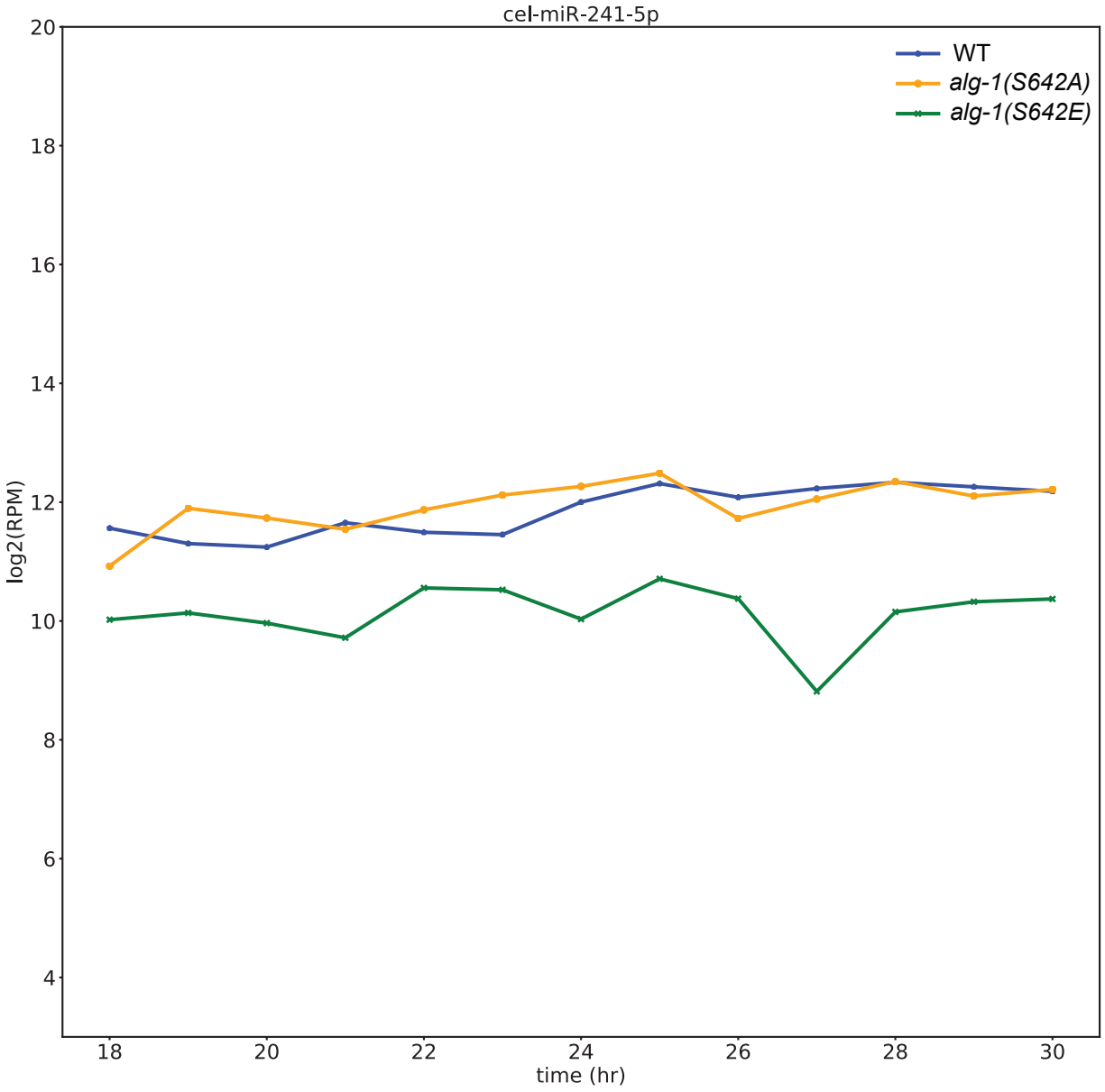
cel-miR-241-5p
WT
alg-1(S642A)
alg-1(S642E)
log2(RPM)
time (hr)
20
18
16
14
12
10
8
6
4
18
20
22
24
26
28
30

Data S1

REFERENCES

[S1] Rüdel, S., Wang, Y., Lenobel, R., Korner, R., Hsiao, H.H., Urlaub, H., Patel, D., and Meister, G. (2011). Phosphorylation of human Argonaute proteins affects small RNA binding. Nucleic Acids Res *39*, 2330-2343. 10.1093/nar/gkq1032.

[S2] Nakanishi, K., Ascano, M., Gogakos, T., Ishibe-Murakami, S., Serganov, A.A., Briskin, D., Morozov, P., Tuschl, T., and Patel, D.J. (2013). Eukaryote-specific insertion elements control human ARGONAUTE slicer activity. Cell Rep 3, 1893-1900. 10.1016/j.celrep.2013.06.010.

[S3] Faehnle, C.R., Elkayam, E., Haase, A.D., Hannon, G.J., and Joshua-Tor, L. (2013). The making of a slicer: activation of human Argonaute-1. Cell Rep 3, 1901-1909. 10.1016/j.celrep.2013.05.033.

[S4] Schirle, N.T., and MacRae, I.J. (2012). The crystal structure of human Argonaute2. Science 336, 1037-1040. 10.1126/science.1221551.

[S5] Elkayam, E., Kuhn, C.D., Tocilj, A., Haase, A.D., Greene, E.M., Hannon, G.J., and Joshua-Tor, L. (2012). The structure of human argonaute-2 in complex with miR-20a. Cell 150, 100-110. 10.1016/j.cell.2012.05.017.

[S6] Schirle, N.T., Sheu-Gruttadauria, J., and MacRae, I.J. (2014). Structural basis for microRNA targeting. Science 346, 608-613. 10.1126/science.1258040.

[S7] Park, M.S., Phan, H.D., Busch, F., Hinckley, S.H., Brackbill, J.A., Wysocki, V.H., and Nakanishi, K. (2017). Human Argonaute3 has slicer activity. Nucleic Acids Res 45, 11867-11877. 10.1093/nar/gkx916.

[S8] Park, M.S., Araya-Secchi, R., Brackbill, J.A., Phan, H.D., Kehling, A.C., Abd El-Wahab, E.W., Dayeh, D.M., Sotomayor, M., and Nakanishi, K. (2019). Multidomain Convergence of Argonaute during RISC Assembly Correlates with the Formation of Internal Water Clusters. Mol Cell 75, 725-740 e726. 10.1016/j.molcel.2019.06.011.

[S9] Sheu-Gruttadauria, J., Xiao, Y., Gebert, L.F., and MacRae, I.J. (2019). Beyond the seed: structural basis for supplementary microRNA targeting by human Argonaute2. EMBO J 38, e101153. 10.15252/embj.2018101153.

[S10] Sheu-Gruttadauria, J., Pawlica, P., Klum, S.M., Wang, S., Yario, T.A., Schirle Oakdale, N.T., Steitz, J.A., and MacRae, I.J. (2019). Structural Basis for Target-Directed MicroRNA Degradation. Mol Cell 75, 1243-1255. 10.1016/j.molcel.2019.06.019.